Available online at www.sciencedirect.com
SCIENCE DIRECT®

Journal of the European Ceramic Society 23 (2003) 2905–2919

www.elsevier.com/locate/jeurceramsoc

Preparation of pHEMA–CP composites with high interfacial adhesion via template-driven mineralization

Jie Song[a,b,*], Eduardo Saiz[a], Carolyn R. Bertozzi[a,b,c,d,*]

[a]*Materials Sciences Division, Lawrence Berkeley National Laboratory, University of California, Berkeley, CA 94720, USA*
[b]*Department of Chemistry, University of California, Berkeley, CA 94720, USA*
[c]*Department of Molecular and Cell Biology, University of California, Berkeley, CA 94720, USA*
[d]*Howard Hughes Medical Institute, University of California, Berkeley, CA 94720, USA*

Abstract

We report a template-driven nucleation and mineral growth process for the high-affinity integration of calcium phosphate (CP) with a poly(2-hydroxyethyl methacrylate) (pHEMA) hydrogel scaffold. A mineralization technique was developed that exposes carboxylate groups on the surface of crosslinked pHEMA, promoting high-affinity nucleation and growth of calcium phosphate on the surface along with extensive calcification of the hydrogel interior. External factors such as the heating rate, the agitation of the mineral stock solution and the duration of the process that affect the outcome of the mineralization were investigated. This template-driven mineralization technique provides an efficient approach toward bonelike composites with high mineral–hydrogel interfacial adhesion strength.

Keywords: Biomedical applications; Heterogeneous nucleation; Hydrogel-CP composite; Interfacial adhesion

1. Introduction

Current artificial materials used in the fabrication of orthopedic implants were originally developed for non-biological applications. Although they could provide an immediate solution for many patients, their long-term outcomes are not satisfactory. This is due to two major limitations: (1) these materials exhibit serious mechanical property mismatches with natural bone tissues;[1] and (2) these materials typically do not bear any functionalities that encourage the communication with their cellular environment, therefore limiting the potential for tissue attachment and in-growth.[2] The development of a new generation of bonelike composite materials with improved mechanical properties and enhanced biocompatibility over traditional implants calls for a biomimetic synthetic approach using natural bone as a guide.

Natural bone is a composite of collagen, a protein-based hydrogel template, and inorganic dahilite (carbonated apatite) crystals. The unusual combination of a hard inorganic material and an underlying elastic hydrogel network endows native bone with unique mechanical properties, such as low stiffness, resistance to tensile and compressive forces and high fracture toughness.[3] Throughout the cavities of bone, there are bone cells and a myriad of soluble factors and extracellular matrix components that are constantly involved with the bone formation and remodeling process.[4] For instance, it is suggested that acidic extracellular matrix proteins that are attached to the collagen scaffold play important templating and inhibitory roles during the mineralization process.[5,6] Presumably, the acidic groups serve as binding sites for calcium ions and align them in an orientation that matches the apatite crystal lattice.[7,8] It is the critical features like these that the biomimetic synthesis of artificial bone should emulate. We hypothesize that this can be realized by the generation of functional polymer scaffolds displaying surface ligands that mimic critical extracellular matrix components known to direct template-driven biomineralization, or to stimulate or assist cell adhesion, proliferation, migration and differentiation.[9–13] Ideally, such 3-dimensional scaffolds should also possess proper physical properties, such as desired porosity and water retention ability, to allow both pre-implantation cell seeding and post-implantation tissue ingrowth.

* Corresponding authors. Tel.: +1-510-486-4125; fax: +1-510-486-4995 (J. Song); +1-510-643-1682; fax: +1-510-643-2628 (C.R. Bertozzi).
E-mail addresses: jsong@lbl.gov (J. Song), bertozzi@cchem.berkeley.edu (C.R. Bertozzi).

0955-2219/03/$ - see front matter © 2003 Elsevier Ltd. All rights reserved.
doi:10.1016/S0955-2219(03)00302-9

Hydrogel polymers are particularly appealing candidates for the design of highly functional tissue engineering scaffolds.[14,15] The intrinsic elasticity and water retention ability of synthetic hydrogels resemble those of natural hydrogels, such as collagen matrices that are prevalent as structural scaffolds in various connective tissues including bone.[14] The porosity of synthetic hydrogels may be controlled by various techniques including solvent casting/particulate leaching,[16,17] phase separation,[18] gas foaming,[19] solvent evaporation,[20] freeze drying,[21] and blending with non-crosslinkable linear polymers[22] to afford a range of mechanical properties. Another important feature of hydrogels is that they can be assembled in 3-dimensional form displaying multiple functional domains through copolymerization of different monomers. The polymerization chemistry is water compatible, allowing incorporation of polar ligands such as anionic peptides that mimic the acidic matrix proteins regulating mineral growth, and biological epitopes such as the tripeptide RGD[23–25] that promote cellular adhesion.

Poly(2-hydroxyethyl methacrylate), or pHEMA, is one of the most well-studied synthetic hydrogel polymers.[26] With its high biocompatibility, pHEMA and its functionalized copolymers have become some of the most widely used synthetic hydrogels in tissue engineering. Applications include ophthalmic devices (e.g. contact lens),[27,28] cartilage replacements,[29] bonding agents in dental resins and bone cements,[30–32] and various drug delivery vehicles.[33,34] One of the major challenges for its application as a 3-dimensional scaffold of artificial bonelike materials, however, is to realize a high-affinity integration of inorganic minerals with the pHEMA-based organic scaffold.

The most widely used existing approach of mineralizing organic polymer films with hydroxyapatite (HA) ($Ca_{10}(PO_4)_6(OH)_2$), a mineral closely related to carbonated apatite, the major inorganic component of natural bone, is the incubation of substrates with simulated body fluid (SBF).[35] This leads to slow growth of crystalline or amorphous biominerals that exhibit poor adhesion and lack a structural relationship with the substrate.[35,36] Recently, chemical treatment of biodegradable poly(lactide-*co*-glycolide) films with aqueous base has been shown to facilitate the growth of crystalline carbonate apatite on the surface.[37] Both the morphology and thickness of the resulting crystalline apatite layer, however, suggest that it is likely to suffer from inadequate interfacial adhesion (between the mineral and the polymer substrate) and poor mechanical properties. Other efforts aimed at improving the interface of HA with polymers include the use of silane coupling agents,[38,39] zirconyl salts,[40] polyacids[41,42] and isocyanates.[43,44] However, to this date, composite materials that integrate HA and organic scaffolds, especially pHEMA-based hydrogels, and demonstrate the level of integration of natural bone, have not yet been achieved.

Here we report the development of a rapid and effective mineralization method that leads to high affinity integration of HA with a pHEMA hydrogel scaffold. This work serves as an important first step towards the development of hydrogel-based biomimetic composite materials. External factors such as heating rate, agitation and the duration of the process that affect the outcome of the mineralization (e.g. the extent of mineralization, the strength of mineral adhesion at the gel–mineral interface and the mineral crystallinity) were investigated.

2. Experimental

2.1. Hydrogel preparation

2-Hydroxyethyl methacrylate (HEMA) was purchased from Aldrich and purified via distillation under reduced pressure prior to use. In a typical procedure, 500 mg of hydrogel monomer was combined with 10 μl of ethylene glycol dimethacrylate, 100 μl of Milli-Q water and 150 μl of ethylene glycol. To this mixture was added 50 μl each of an aqueous solution of sodium metabisulfite (150 mg/ml) and ammonium persulfate (400 mg/ml). The well-mixed viscous solution was then poured into a glass chamber made by microscope slides and allowed to stand at room temperature overnight. The gels (5.5 cm × 1.5 cm × 1 mm) were then soaked in Milli-Q water for 2–3 days, with daily exchange of fresh water, to ensure the complete removal of unreacted monomers before they were used for mineralization and further physical characterizations.

2.2. Equilibrium water content (EWC) measurements

The EWC at room temperature is defined as the ratio of the weight of water absorbed by a dry hydrogel to the weight of the fully hydrated hydrogel. The amount of water absorbed by the hydrogel is determined from the weight of a freeze-dried gel (Wd) and the weight of the corresponding hydrated gel (Wh) according to the following equation:

$$\mathrm{EWC}\ (\%) = [(\mathrm{Wh} - \mathrm{Wd})/\mathrm{Wh}] \times 100$$

2.3. Contact angle measurements

The contact angles of diiodomethane droplets against water on hydrogels were measured using the sessile drop method. A 3–5 μl droplet of diiodomethane was placed on the surface of a segment of hydrogel submerged in water. The static contact angles were measured with a Goiniometer from both sides of the droplet within 10 s after depositing the drop, and the values were averaged.

The contact angle was found to be 129 and 142° for the pre-hydrolyzed pHEMA and post-hydrolyzed pHEMA, respectively.

2.4. Mineralization of hydrogels with the urea-mediated process

HA (2.95 g) was suspended into 200 ml of Milli-Q water with stirring, and 2 M HCl was added sequentially until all the HA suspension was dissolved at a final pH of 2.5–3. Urea (24 g) was then dissolved into the solution to reach a concentration of 2 M. Each hydrogel strip (5.5 cm × 1.5 cm × 1 mm) was then immersed into 50 ml of the acidic HA–urea stock solution. The solution was slowly heated with a commercial hot plate (Corning hot plate/stirrer model PC-420) to 90–95 °C (within 2 h, with an average heating rate about 0.6 °C/min) without agitation of the mineralization solution and maintained at that temperature overnight when necessary (for preparation of composites with thicker CP layers). The final pH was around 8.

For the investigation of the effect of different heating rates, a homemade heating system with fine temperature control was employed. The system was assembled with a mineral oil bath, a stirring plate, a temperature controller (Eurotherm model 808), a Glo-quartz® immersion heater (immersed in the mineral oil bath) and a K-type thermocouple. Each hydrogel strip (1.0 cm × 1.5 cm × 1 mm) was immersed into a scintillation vial containing 15 ml of the acidic HA–urea stock solution. The scintillation vial was then loosely capped and heated in the mineral oil bath with heating rates controlled at 1.0, 0.5, 0.2 and 0.1 °C/min. Magnetic stirring was applied to the oil bath rather than the HA–urea mineralization solution.

The same experimental setup was used for the investigation of the effect of agitation of mineralization solution, where hydrogels were attempted for mineralization with heating rates at 1.0, 0.5, 0.2 and 0.1 °C/min, under constant stirring of the acidic HA–urea stock solution.

2.5. Structural characterizations

Mineralized hydrogel strips were repeatedly washed in water to remove loosely attached minerals and soluble ions before they were freeze-dried for further structural analyses and mechanical characterization. The surface microstructures and crystallinity of the materials grown on the surface and inside of the hydrogel were analyzed by scanning electron microscopy (SEM) with associated energy dispersive spectroscopy (EDS) and X-ray diffraction (XRD).

2.5.1. SEM–EDS

All SEM micrographs of freeze-dried hydrogels and hydrogel–mineral composites were obtained with a ISI-DS 13OC dual stage SEM with associated EDS. Samples were either coated with Au or Pt on a BAL-TEC, SCD 050 sputter coater to achieve optimal imaging results, or coated with carbon for EDS analysis. The imaging and analysis of composite materials were performed at 15 kV, and those of hydrogels were performed under reduced voltage (10 kV). The determination of Ca/P ratios of all composite materials were based on calibration using a standard synthetic HA sample.

2.5.2. XRD

The presence and overall orientation of crystalline phases in the precipitated mineral layers were evaluated by XRD with a Siemens D500 instrument using Cu Kα radiation.

2.5.3. Evaluation of mineral–hydrogel interfacial adhesion

In order to evaluate the adherence of the mineral layers attached to pHEMA hydrogels, the relative crack resistance was qualitatively evaluated by indentation.[45–47] The indentation test was performed on the freeze-dried composite using a Vickers indentor (Micromet, Buehler, Ltd., USA). Loads from 5 to 15 Newtons were applied for 20 s for each measurement. After indentation, the samples where analyzed by SEM in order to check for delamination. Lack of delamination is an indication of strong adhesion between the mineral layer and the hydrogel substrate.

3. Results and discussions

A standard radical polymerization protocol[48] was applied for the preparation of poly(2-hydroxyethyl methacrylate) (pHEMA) hydrogels crosslinked with 2% (by weight) ethylene glycol dimethacrylate (EGDMA). The gels were found to have 40% EWC.

Calcium apatites are known to promote bone apposition and differentiation of mesenchymal cells to osteoblasts.[49] In this work, synthetic HA was used in the fabrication of hydrogel-based bonelike composite materials. HA has limited solubility in water at neutral and basic pH but is highly soluble at acidic pH.[50] Based on this property, we employed a urea-mediated solution precipitation technique that was previously used in the preparation of composite ceramic powders.[51,52] In an adapted protocol, a segment of pHEMA hydrogel was soaked in an acidic solution (pH 2.5–3) of HA containing a high concentration of urea (2 M). Upon gradual heating (without stirring) from room temperature to 90–95 °C (heating time 2 h, with an average heating rate around 0.6 °C/min), urea started to decompose and the pH slowly increased (around pH 8). Under these conditions, some hydrolysis of the 2-hydroxyethyl esters

occurred, promoting heterogeneous nucleation and 2-dimensional growth of a thin calcium phosphate (CP) layer at the hydrogel surface.

The hydrolysis of 2-hydroxyethyl esters during the thermo-decomposition of urea was expected to lead to an increase of surface hydrophilicity, which was confirmed by contact angle and EWC measurements. In a mock experiment, a segment of pHEMA gel was thermally treated as described above in a solution containing the same concentration of urea, without the presence of HA. Diiodomethane, a hydrophobic solvent that is known to from stable droplets on hydrophilic materials without noticeable penetration and contact angle hysteresis,[53] was used for measuring contact angles against water on both the treated and untreated pHEMA gels. The contact angle of a diiodomethane droplet on the gel surface was found to increase from 129 to 142° upon the urea-mediated thermal treatment for 2 h. The observed decrease in surface wettability by a hydrophobic solvent is consistent with the postulated in situ generation of polar surface carboxylates during the urea-mediated mineralization. The hydrolysis also led to a slight increase (2–3%) in the EWC of the gel.

The strong affinity between calcium and the in situ generated acidic surface of pHEMA led to the 2-dimensional outward growth of calcium phosphate from individual nucleation sites (the bright centers indicated by arrows in Fig. 1A and C). After 2 h, the circular mineral layers merged and covered the entire surface (Fig. 1A and C). The merge of circularly grown mineral layers resulted in sharp edges connecting individual CP patches (Fig. 1B and D). The calibrated EDS area analysis performed on the mineral surface of the composite revealed a Ca/P ratio (1.6 ± 0.1) similar to that of synthetic HA (Fig. 1E).

XRD analysis performed on the mineralized pHEMA composite indicated that the calcium phosphate layer was either nanocrystalline or amorphous. No typical reflections for crystalline HA were observed, with only a few broad reflections [Fig. 1F, (a)] similar to those observed in the hydrogel prior to mineralization [Fig. 1F, (b)]. This suggests that although there is high affinity binding between calcium ions and the in situ generated surface carboxylates, the spacing, order and/or alignment of these surface anionic ligands do not promote the epitaxial growth of large calcium apatite crystallites along any particular orientation.

The adhesion strength of the CP layer to the gel surface was qualitatively evaluated by microindentation analysis[45–47] performed on the surface of the freeze-dried hydrogel–CP composite. During the freeze-drying process, the hydrogel substrate shrunk more than the surface mineral layer, resulting in a slight bending of the composite. However, such bending did not lead to the dissociation of the mineral layer from the hydrogel substrate. No delamination of the mineral layer was observed by SEM (Fig. 2) even after Vickers indentations with loads up to 15 N. Neither the center nor the tip of the indenter markers with loads of 5 N (Fig. 2B and C) and 10 N (Fig. 2D) showed any signs of delamination of the CP layer which is an indication of good adhesion at the mineral–gel interface. This represents a major improvement over the widely used SBF mineralization method.

Most of the flake-like crystal apatite coatings obtained by mineralization in SBF on bioactive glasses, polymer scaffolds or collagen films are not robust and tend to delaminate easily upon drying.[35,36,54,55] We attempted microindentation analysis with the apatite layers formed on bioglass using SBF mineralization.[55] The minerals crumbled with even very low loadings and are therefore considered not amendable for such analysis. Recently, a modified mineralization approach, involving the use of very high concentrations of SBF and careful control of HCO_3^- concentrations, was used to bind nano-sized apatite crystals to commercial metal implants with improved strength.[56,57] However, no mechanical tests that could characterize the interfacial adhesion between these apatites and the metal substrates was reported.

Overall, there are several notable features of this mineralization procedure. First, increasing pH and temperature during the process promotes the hydrolysis of the ethyl ester side chains of pHEMA and leads to the in situ generation of an acidic surface and a partially acidic interior that has high affinity for calcium ions. Simultaneously, the mineral concentration in the solution undergoes a dramatic change (as the pH rose from 3 to 8) as depicted by the dotted curve shown in Fig. 3, where Curve 1 is adapted from the work of Nancollas et al., depicts the general solubility of hydroxyapatite.[50] Curves 2 and 3 represent qualitative depictions of typical nucleation behavior of calcium phosphates derived from basic nucleation theory reported in the literature.[51,52] The subtle differences in solubility and precipitation behavior of various calcium phosphates are not reflected in this scheme. The high affinity between the calcium ions and the exposed carboxylate groups at the gel surface translates into a low interfacial energy between the hydrogel and calcium phosphate, and consequently, a low energy barrier for the heterogeneous nucleation of mineral on the hydrogel surface (as shown by curve 2 in Fig. 3). Second, the thermo-decomposition of urea allows a homogeneous variation of pH across the solution, avoiding a sudden local pH change that is commonly observed with strong base-induced heterogeneous precipitation.[52] Third, any homogeneous precipitates that fall on the hydrogel and remain loosely attached to the composite surface can be easily washed away during the workup rinsing.

To evaluate the reproducibility of this methodology, we investigated how external factors may affect the

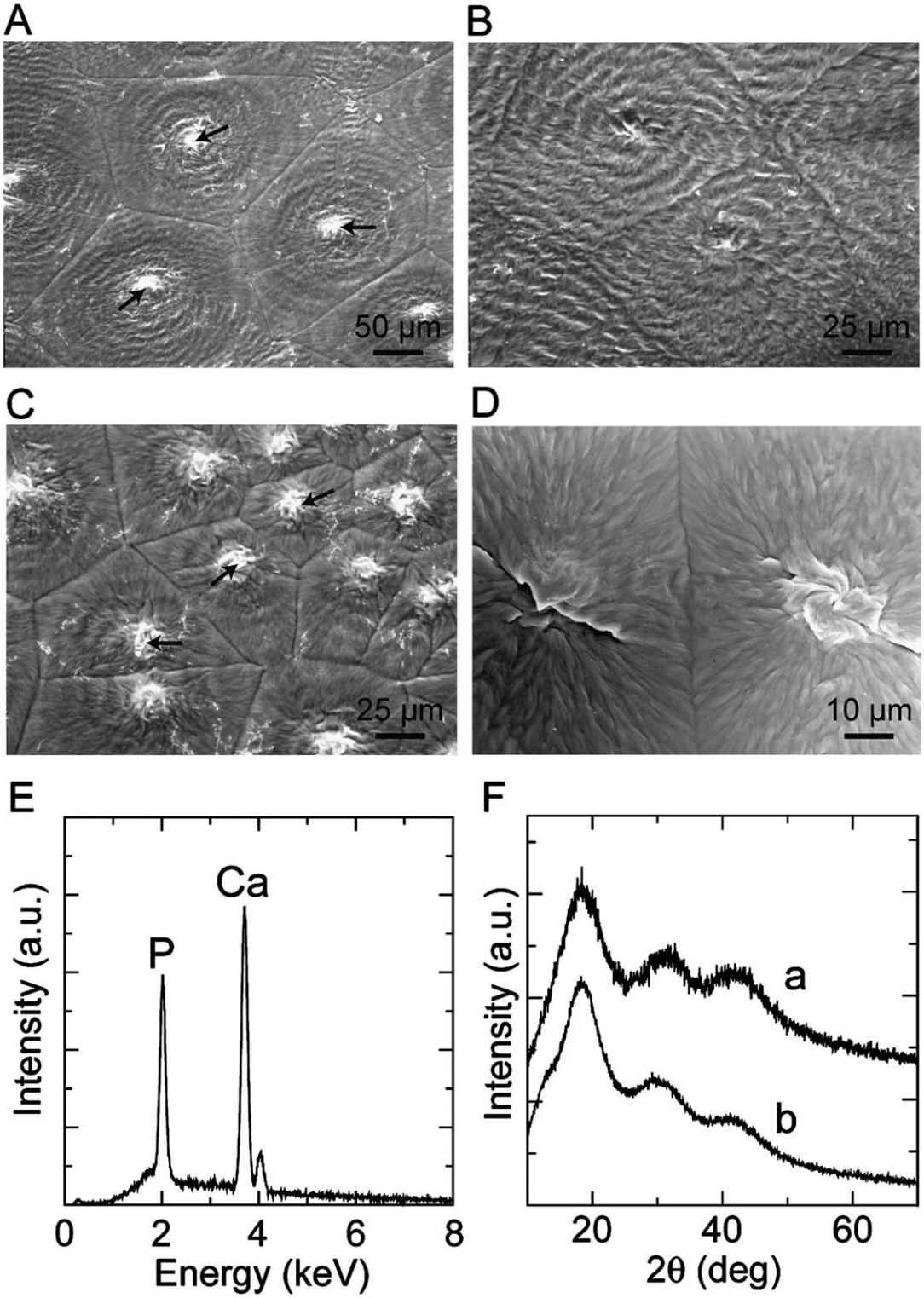

Fig. 1. Morphology and crystallinity of calcium phosphate layer grown on the surface of pHEMA via the urea-mediated process (heating time 2 h, with an average heating rate around 0.6 °C/min). (A) SEM showing 2-dimensional circular outward growth of mineral layers from multiple nucleation sites (indicated by arrows) on the acidic surface of pHEMA. Note the full coverage of the hydrogel surface with mineral layers and the sharp edges connecting neighboring domains. (B) SEM showing the merge of circular mineral domains. (C) SEM showing a different pattern of 2-dimensional circular outward growth of mineral layers from multiple nucleation sites (indicated by arrows) on the acidic surface of pHEMA. Note the full coverage of the hydrogel surface with mineral layers and the sharp edges connecting neighboring domains. (D) SEM showing the merge of two circular mineral domains and the formation of a sharp edge between them. (E) SEM-associated EDS area analysis of the mineral layer shown in micrograph A, confirming the chemical composition and Ca/P ratio (1.6±0.1) that is typical for HA. (F) X-ray diffraction patterns of the pHEMA composite (a) and unmineralized pHEMA gel (b). The lack of diffraction peaks suggests that an amorphous or nanocrystalline layer was formed on the pHEMA surface.

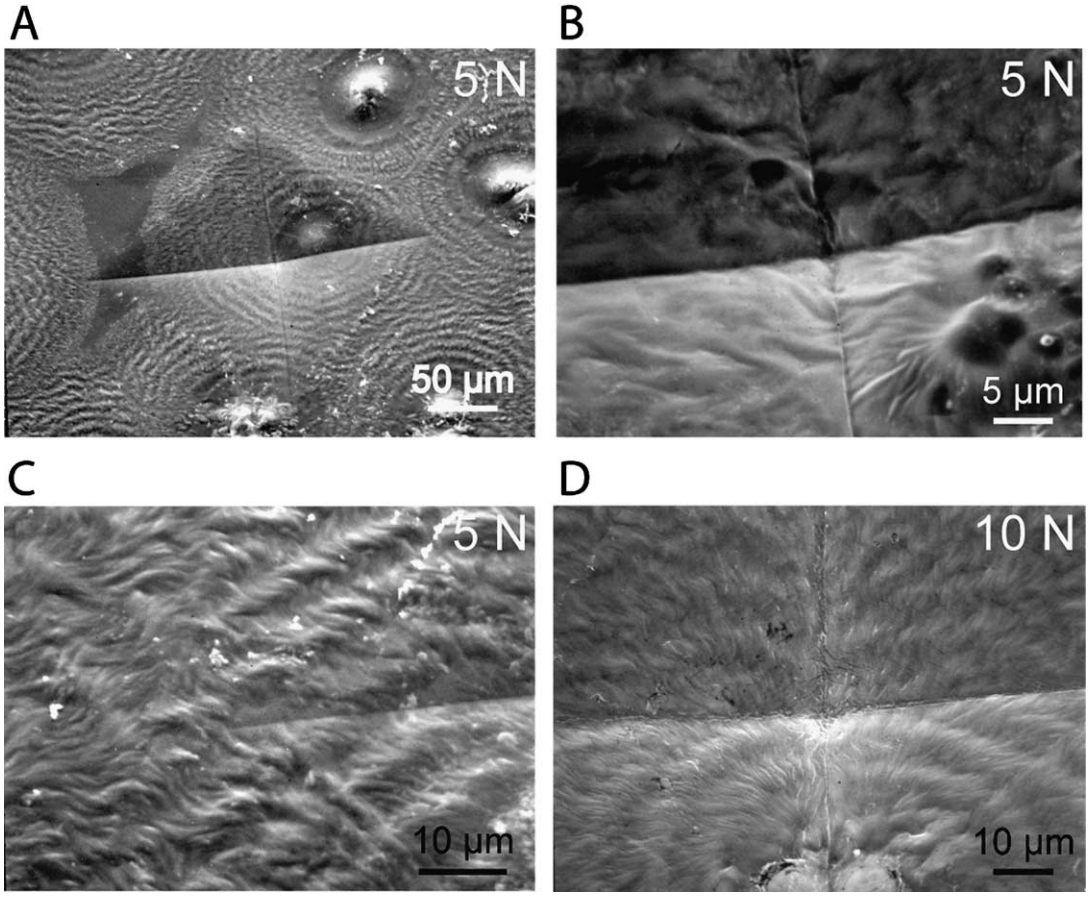

Fig. 2. Microindentation analyses of the mineral–gel interfacial affinity of calcium phosphate layer grown on the surface of pHEMA via the urea-mediated process (heating time 2 h, with an average heating rate around 0.6 °C/min). (A) SEM showing an indent formed on the surface of mineralized pHEMA using a Vickers microindenter with a load of 5 N. The calcium phosphate layer did not delaminate. (B) SEM showing the center of an indent formed on the surface of mineralized pHEMA using a Vickers microindenter with a load of 5 N. (C) SEM showing the tip of an indent formed on the surface of mineralized pHEMA using a Vickers microindenter with a load of 5 N. (D) SEM showing the center of an indent formed on the surface of mineralized pHEMA using a Vickers microindenter with a load of 10 N. The calcium phosphate layer did not delaminate.

outcome of the gel–CP composite formation. Specifically, we monitored the influence of the heating rate, the agitation of the mineral stock solution and the duration of the process. We postulate that these factors should have a direct impact on the in situ generation of acidic calcium-binding sites (or mineral nucleation sites) on the gel surface, the nucleation and precipitation behavior of the mineral (homogeneous vs. heterogeneous nucleation), and the extent (thickness) of mineral coverage on the hydrogel surface, respectively.

Using a homemade heating system with fine temperature control, pHEMA gels were mineralized using the same acidic HA–urea stock solution from room temperature to 95 °C with heating rates of 1.0, 0.5, 0.2 and 0.1 °C/min, respectively. No agitation of the mineral stock solution was applied and the mineralization process was terminated once the temperature reached 95 °C. The resulting composites were then examined for surface mineralization patterns via SEM, elemental compositions via EDS and crystallinity of the mineral components via XRD.

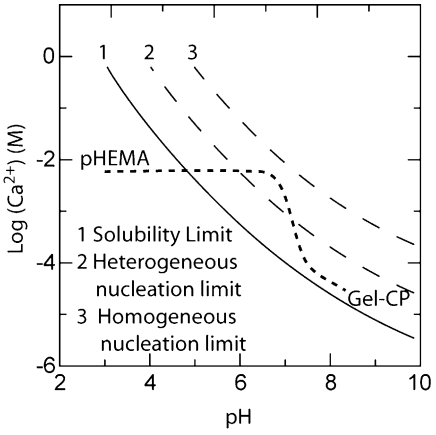

Fig. 3. A qualitative depiction of the urea-mediated, pH-dependent HA nucleation and growth behavior. A proposed urea-mediated, pH-dependent HA nucleation and growth behavior from the solution is qualitatively depicted by the dotted curve, guiding the chemical and physical transformation of the pHEMA hydrogel to a highly integrated Gel-CP composite. Curve 1, the solubility of HA, was adapted from Ref. 46. Curves 2 and 3 represent qualitative depictions of typical nucleation behavior of calcium phosphates derived from basic nucleation theory.

As shown in Fig. 4, a relatively fast heating rate such as 1.0 °C/min did not lead to a level of mineralization of the pHEMA gel that was detectable by either SEM (Fig. 4A and B) or the associated EDS analysis (Fig. 4C). The random and featureless deposits on the hydrogel surface (Fig. 4A) did not correspond to any crystalline calcium apatites as evidenced by the XRD analysis that lacks characteristic reflections of calcium phosphates (Fig. 4D). The EDS analysis performed over the composite using an acceleration voltage of 15 kV led to immediate damage of the surface. Such high surface sensitivity to the electron beam is typical for unmineralized hydrogels. Overall, these data suggests that a fast heating rate such as 1.0 °C/min and insufficient mineralization time (a total of 70 min linear heating from room temperature to 95 °C) do not lead to adequate mineralization of the hydrogel using the urea-mediated protocol described above.

When a 0.5 °C/min heating rate was applied, the formation of circular mineral layers on the hydrogel surface was observed (Fig. 5 A), with similar 2-dimensional outward growth pattern formed around individual nucleation sites (Fig. 5B). X-ray elemental mapping of Ca and P (Fig. 5C and D) showed that the circular mineral patterns were composed of uniform calcium phosphate. EDS analysis performed on the composite revealed a Ca/P ratio matching that of HA (Fig. 5E). XRD of the composite, however, showed no reflections (Fig. 5F) matching with those of crystalline calcium apatites, suggesting that the circular CP layer grown on

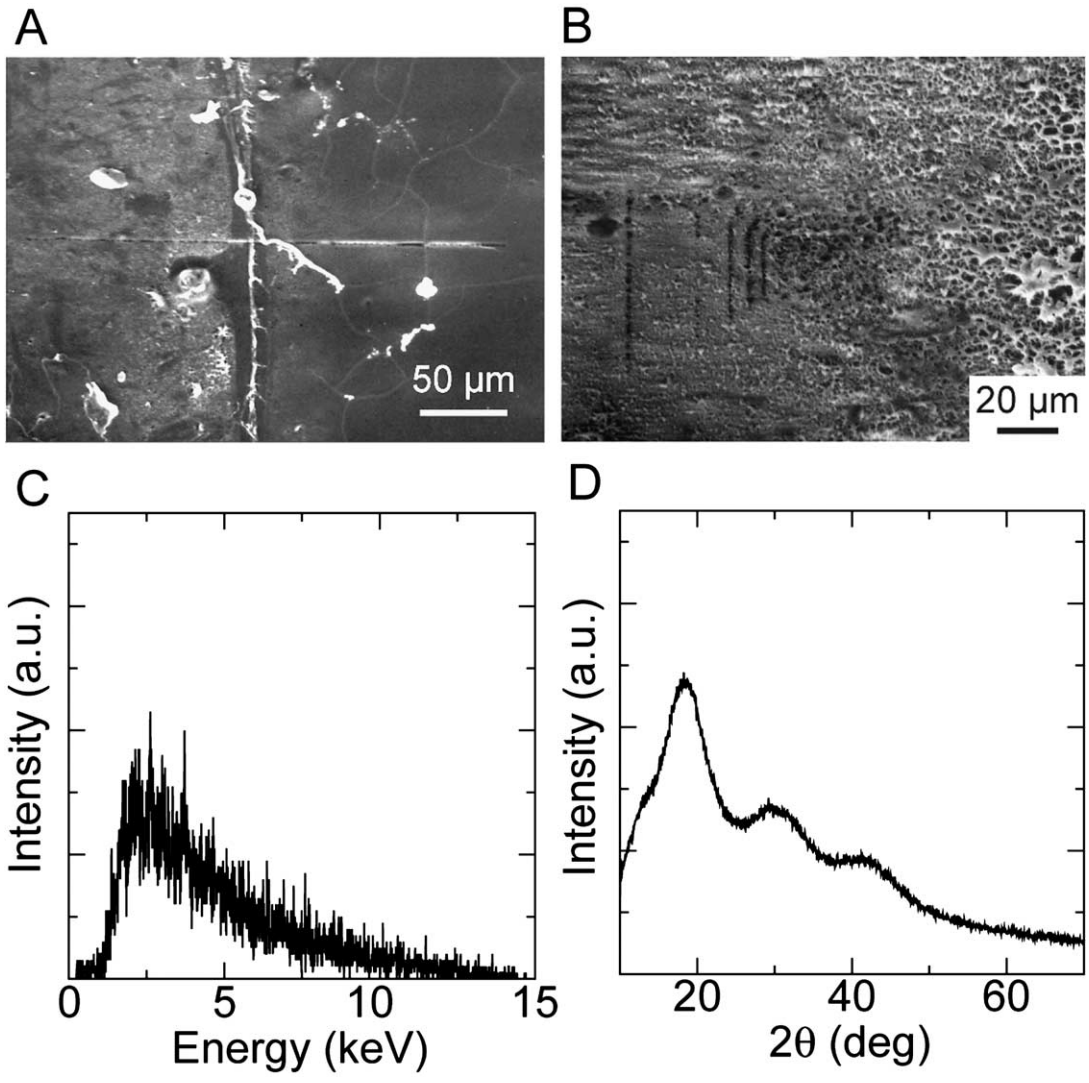

Fig. 4. Mineralization (without agitation) of pHEMA via the urea-mediated process with a linear heating rate of 1.0 °C/min from room temperature to 95 °C. (A) SEM showing the surface morphology of the resulting composite. Note the sporadic irregular precipitates on the hydrogel surface. (B) SEM showing the surface morphology of the resulting composite. Note the damages (dark lines) caused by the electron beams on the hydrogel surface. (C) SEM-associated EDS area analysis of the surface shown in micrograph B. Note the negligible degree of mineralization at the pHEMA gel surface. (D) X-ray diffraction pattern of the resulting composite. The lack of characteristic diffraction peaks of calcium apatites is in agreement with the lack of surface mineral growth under this experimental condition suggested by EDS data.

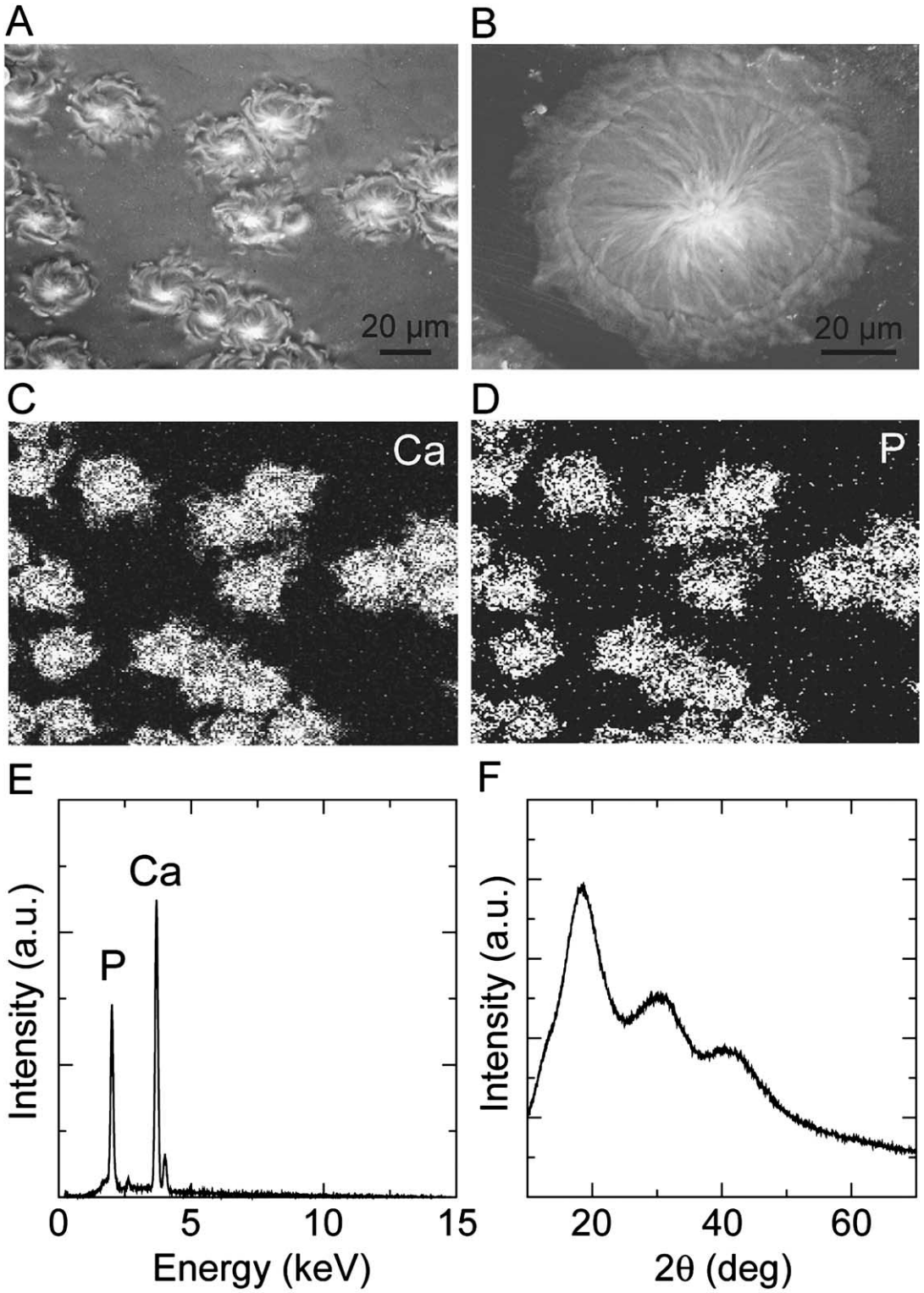

Fig. 5. Mineralization (without agitation) of pHEMA via the urea-mediated process with a linear heating rate of 0.5 °C/min from room temperature to 95 °C. (A) SEM showing 2-dimensional outward growth of mineral rings from multiple nucleation sites on the acidic surface of pHEMA. (B) SEM showing a close-up view of a circular mineral domain. (C) X-ray elemental mapping of Ca with the same sample area shown in micrograph A. (D) X-ray elemental mapping of P with the same sample area shown in micrograph A. (E) SEM-associated EDS area analysis performed over the circular mineral domain shown in micrograph B, confirming the chemical composition and Ca/P ratio of the surface mineral that is typical of HA. (F) X-ray diffraction pattern of the resulting composite. The lack of diffraction peaks suggests that the mineral domains formed on the pHEMA surface were either amorphous or nanocrystalline in nature.

the hydrogel surface were either nanocrystalline or amorphous in nature.

When the linear heating rate (from room temperature to 95 °C) was lowered to 0.2 °C/min, the surface of the hydrogel–mineral composite was fully covered with well-merged circular mineral layers (Fig. 6A and C). Scratching the surface mineral layer with a razor blade (Fig. 6C) did not lead to any delamination, indicating good adhesion strength at the gel–mineral interface. In addition, we observed the growth of HA crystals forming spherical aggregates on top of the initial nucleation sites (centers of circular mineral rings). These mineral spheres are composed of plate-like crystallites (Fig. 6D), a typical morphology observed with the crystalline apatite grown on bioactive glasses, polymer substrates or collagen films using SBF mineralization.[35–37,55] EDS analysis performed on the spherical apatite aggregates (Fig. 6E) and XRD performed on the composite material (Fig. 6F) confirmed the expected Ca/P ratio and typical reflections, (002) and (112), for crystalline HA.[55] Our results so far suggest that a lower heating rate and a more sufficient overall mineralization time promote the formation of better-merged CP layers on the gel surface. And once the gel surface is fully covered with the initial nanocrystalline or amorphous CP layer, large platelet crystallites of CP, easily detectable by XRD, start to grow on top of the initial nucleation sites.

The slowest linear heating rate we attempted for the current investigation was 0.1 °C/min (from room temperature to 95 °C). The most pronounced feature resulted from this mineralization condition was the dramatic increase of the number of nucleation sites formed on the pHEMA hydrogel surface (Fig. 7A – D). The longer exposure of the pHEMA gel to any given pH during the urea-mediated process is likely to lead to a more sufficient hydrolysis of the ethyl ester side chains, resulting in increased numbers of surface carboxylates that could serve as tight calcium ion binders and initial nucleation sites. The overwhelming amount of nucleation sites (the bright spots shown in Fig. 7A and C) also made the distinction of 2-dimensional outward growth of circular CP layers difficult. A high-resolution image of some separate nucleation sites before they merge with each other, however, unequivocally showed the 2-dimensional outward growth pattern around these nucleation centers (Fig. 7D). X-ray elemental mapping of Ca and P (Fig. 7E and F) again showed that the observed mineral patterns were composed of uniform calcium phosphate. EDS area analysis performed on the mineral surface shown in the inset of Fig. 7A revealed a Ca/P ratio matching that of HA. XRD of the composite showed typical reflections (inset of Fig. 7B) matching with those of crystalline calcium apatites. This is likely to result from the formation of crystalline aggregates of plate-like HA (Fig. 7B) that were found over some nucleation sites within areas fully covered with amorphous CP layers.

The influence of the agitation of the HA–urea mineral stock solution on the nucleation and precipitation behavior of the mineral was investigated using the same range of heating rates described above. Upon constant stirring of the mineralization solution, HA were found to homogeneously precipitate out of the mineral solution with the gradual increase of pH. No nucleation and high-affinity growth of calcium apatites on the pHEMA gel surface was observed with any tested heating rates under constant agitation. This suggests that direct stirring of the HA–urea mineral stock solution interferes with the desired heterogeneous nucleation and growth of CP on the in situ generated acidic gel surface. Instead, it promotes homogeneous precipitation of HA across the solution, resulting in the formation of large amount of HA precipitates.

Finally, we examined the possibility of forming thicker CP layers over the pHEMA gel surface by extending the mineralization time for another 10–12 h after reaching 95 °C. Indeed, mineral coatings with thicknesses up to several microns were obtained, with good integration at the mineral–gel interface as shown in a cross-section image of the composite (Fig. 8A). The growth of spherical HA crystal aggregates on top of initial nucleation sites was again observed (Fig. 8B). These mineral spheres are composed of plate-like crystallites as shown in the insert of Fig. 8B. EDS analysis performed on the spherical apatite aggregates confirmed the expected Ca/P ratio (1.6 ± 0.1) and XRD confirmed the crystalline nature of these plate-like HA, with typical reflections of (002) and (112) (Fig. 8C and D). The cross-section examination of the composite material revealed that there were significant degrees of calcium accumulation inside the hydrogel as well, although the degree of phosphate incorporation was limited (Fig. 8E and F). The accumulation of calcium ions in the hydrogel interior may be promoted by the partial hydrolysis of the 2-hydroxyethyl ester side chains inside the pHEMA gel. The growth of calcium apatites inside the pHEMA scaffold is limited by both the space (note that no special technique was applied to promote the formation of a porous hydrogel scaffold in the current study) and the concentration of free anions achieved inside the already partially anionic hydrogel.

4. Summary

The mineralization method we describe here takes advantage of the dramatically different solubilities of HA in acidic and basic aqueous solutions and the chemically labile nature of ester groups of pHEMA in basic solutions. We employed thermo-decomposition of urea in aqueous media as a facile pH modulator to generate an anionic surface and partially acidic interior of the pHEMA gel. This initiated the heterogeneous nuclea-

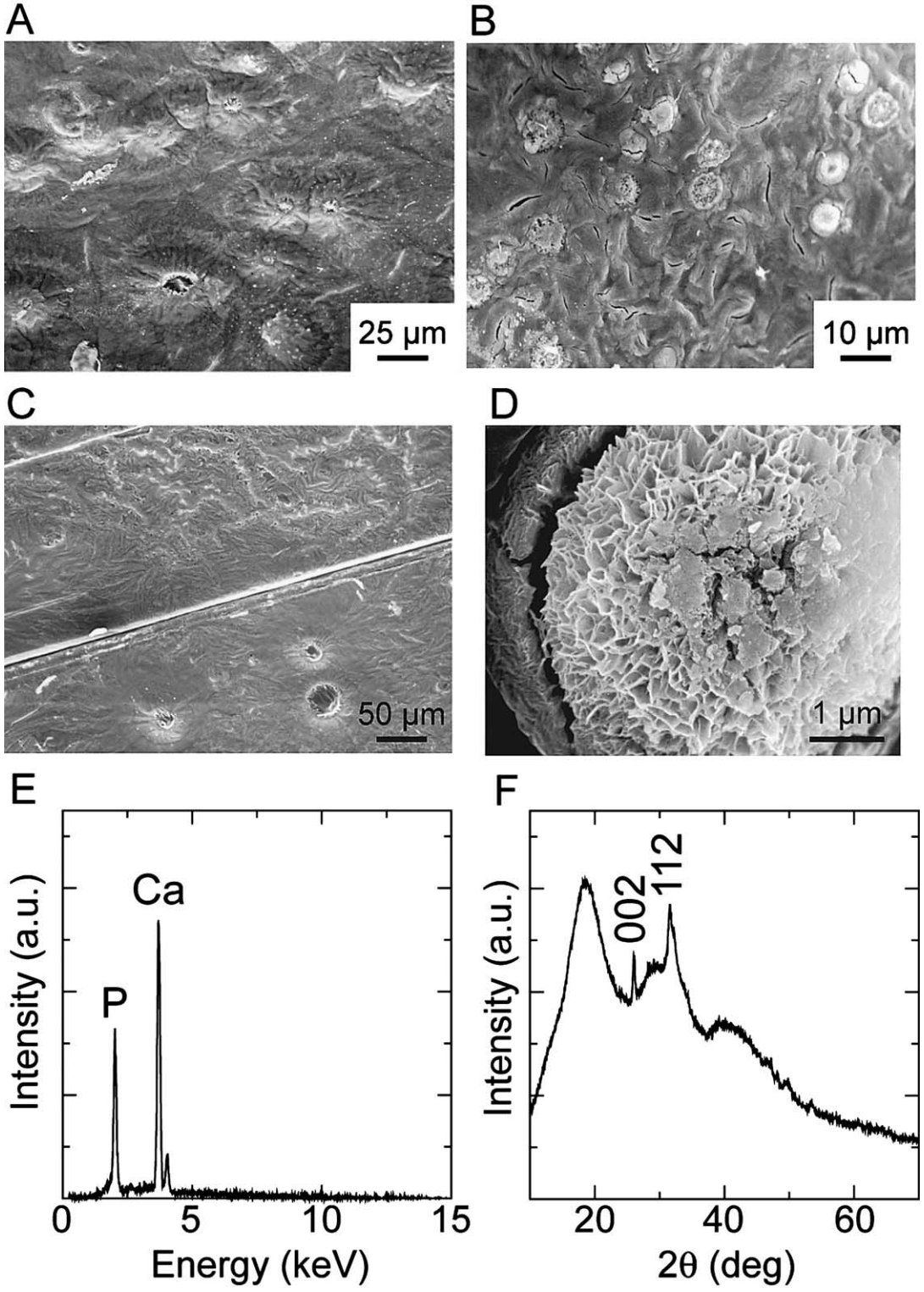

Fig. 6. Mineralization (without agitation) of pHEMA via the urea-mediated process with a linear heating rate of 0.2 °C/min from room temperature to 95 °C. (A) SEM showing 2-dimensional circular outward growth of mineral layers from multiple nucleation sites on the acidic surface of pHEMA. Note the full coverage of the hydrogel surface with the mineral layer. (B) SEM showing 2-dimensional circular outward growth of mineral layers from multiple nucleation sites on another area of the acidic surface of pHEMA. (C) SEM showing a fully mineralized surface scratched with a razor blade. Note that no delamination of the mineral layer was observed around the scratches. (D) SEM showing an expanded view of one spherical cluster of calcium apatite crystallites located at the center of the mineral rings (on top of the initial nucleation sites). Note the platelike morphology of the calcium apatite crystallites that is commonly observed with crystalline apatites grown on various substrates during SBF mineralization. (E) SEM-associated EDS area analysis of the mineral layer shown in micrograph A, confirming the chemical composition and Ca/P ratio that is typical for HA. (F) X-ray diffraction patterns of the composite. Peaks corresponding to crystalline HA were indexed, confirming the crystalline nature of the spherical HA aggregates shown in micrograph D.

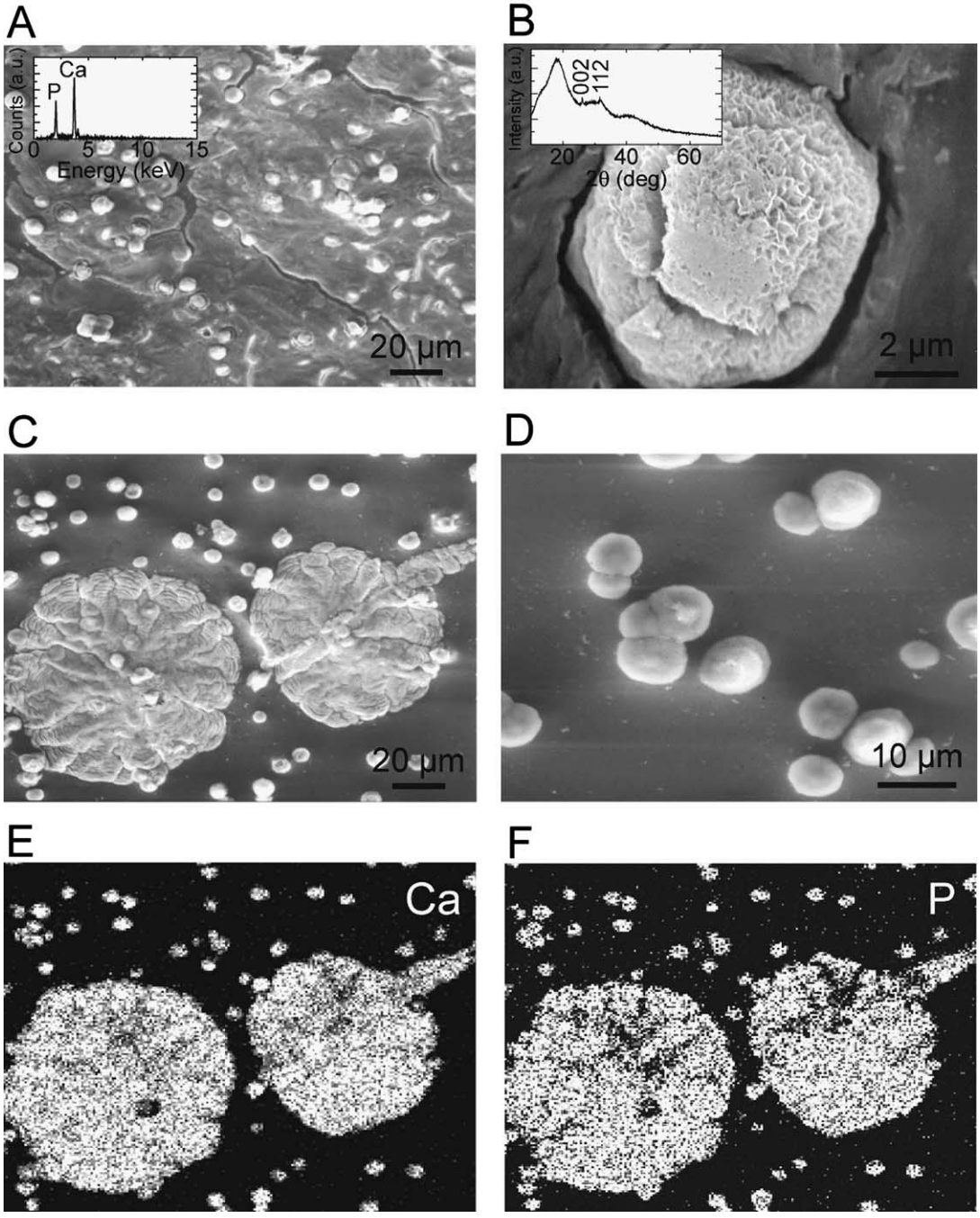

Fig. 7. Mineralization (without agitation) of pHEMA via the urea-mediated process with a linear heating rate of 0.1 °C/min from room temperature to 95 °C. (A) SEM showing the full coverage of mineral layers on the surface of a pHEMA gel. Note the overwhelming amount of nucleation sites scattered throughout the merged mineral domains. The inset shows the EDS area analysis performed over the same fully mineralized surface, confirming the chemical composition and Ca/P ratio that is typical for HA. (B) SEM showing an expanded view of one spherical cluster of plate-like calcium apatite crystallites on top of an initial nucleation site. The inset shows X-ray diffraction patterns of the composite. Peaks corresponding to crystalline HA were detected, and are likely to arise from the crystalline spherical HA aggregates shown in micrograph B. (C) SEM showing two calcium phosphate domains grown on the pHEMA gel surface, along with multiple nucleation sites that are yet to be expanded. (D) SEM showing an expanded view of multiple nucleation sites formed over the pHEMA gel surface that were on the verge of further 2-dimensional outward growth and expansion. (E) X-ray elemental mapping of Ca with the same sample area shown in micrograph C. (D) X-ray elemental mapping of P with the same sample area shown in micrograph C.

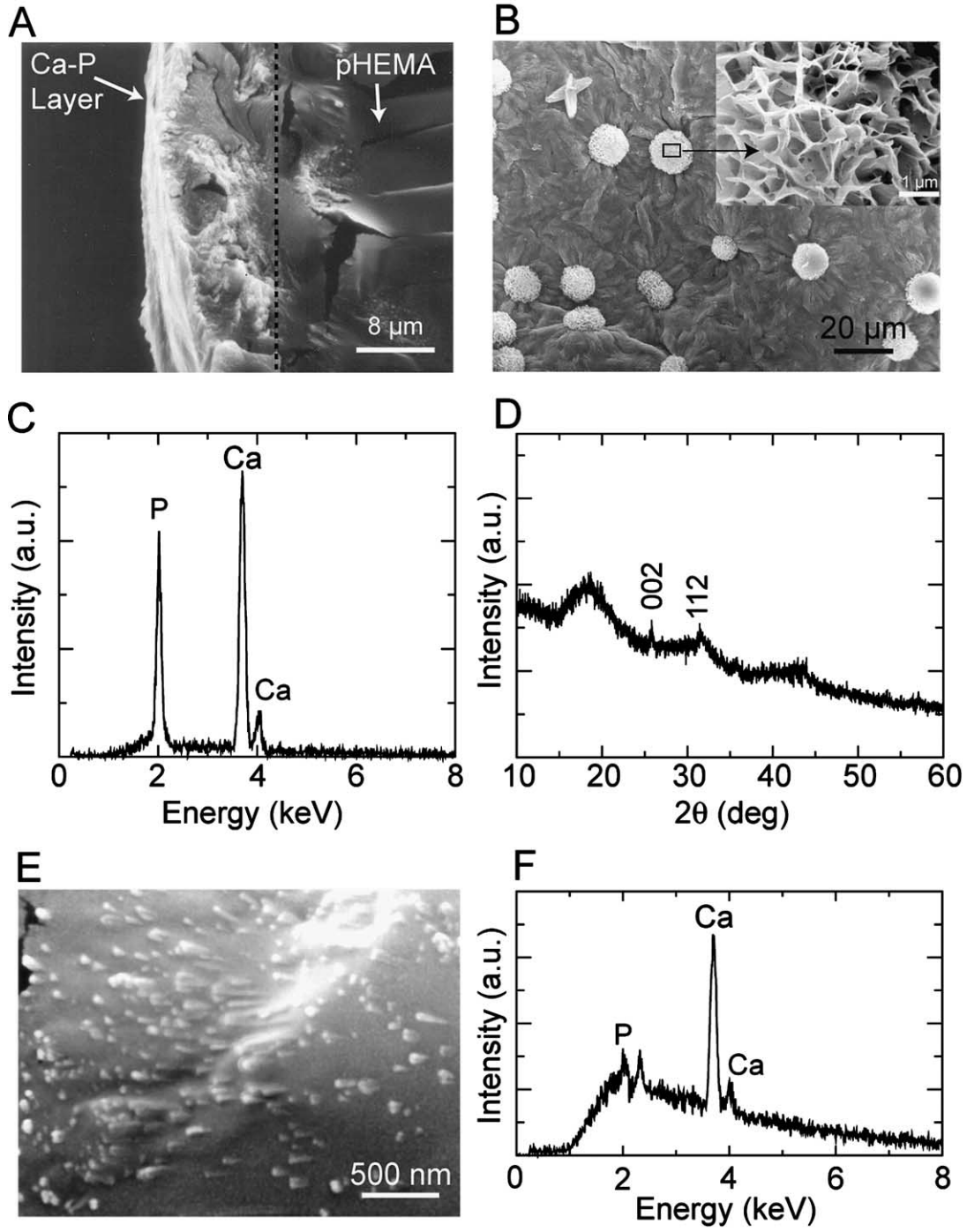

Fig. 8. Extended mineralization (10 h after reaching 95 °C) of pHEMA via a urea-mediated process: morphology, crystallinity and thickness of calcium phosphate layer grown on the hydrogel surface and the calcification of the hydrogel interior. (A) SEM showing the view of a cross-section of the pHEMA–mineral composite after extended mineralization. The sample stage was tilted 45°. Note the micron scale thickness of the mineral layer and the fine integration at the mineral–gel interface. (B) SEM showing fully mineralized surface of pHEMA after extended mineralization, along with the growth of spherical clusters of crystalline HA from nucleation sites located at the centers of circular mineral layers. The inset shows an expanded view of one spherical cluster of HA crystallites. Note the plate-like morphology of the calcium apatite crystallites that is commonly observed with crystalline apatites grown on various substrates during SBF mineralization. (C) Calibrated EDS area analysis of the surface mineral layer shown in micrograph B, confirming the chemical composition and Ca/P ratio (1.6 ± 0.1) that is typical of HA. Same result was obtained on the selected area analysis performed on plate-like HA shown in the inset of micrograph B. (D) X-ray diffraction pattern of the resulting pHEMA–CPcomposite. Peaks corresponding to crystalline HA were detected, suggesting the crystalline nature of the spherical HA grown on top of the calcium phosphate coating. (E) SEM showing the hydrogel interior of the pHEMA–mineral composite. (F) SEM-associated EDS area analysis of the cross-section of pHEMA–apatite composite shown in micrograph E, suggesting significant calcium accumulation throughout the hydrogel interior.

tion and high-affinity growth of calcium apatite on the gel surface and extensive calcification inside the gel. Overall, this method provides a fast and convenient approach for producing robust pHEMA–calcium apatite composite materials with high quality interfacial integration between the mineral and the polymer substrate. Furthermore, this approach provides a foundation for integrating high-affinity template-driven biomineralization with the versatile properties of 3-dimensional hydrogel scaffolds, and opens the door for future application of pHEMA in the design of functionalized bone replacements.

The formation of the robust CP layer on the hydrolyzed surface of pHEMA gel is driven by the lower interfacial energy between the carboxylate rich gel surface and the mineral. Once the gel surface is fully covered with an initial nanocrystalline or amorphous CP layer, large platelets of crystalline apatite grow over the initial nucleation sites. Maintaining the final pH of the mineralization solution at around 8 prevents competing homogeneous precipitation from the medium.

The intrinsic chemical nature of the hydrogel surface (the in situ generation of surface carboxylates that strongly bind to calcium ions) dictates the high-affinity template-driven mineralization described here. By contrast, the formation of loosely covered crystalline mineral layers by conventional SBF mineralization approaches[35,55] indicates limited substrate–mineral interaction. That is, such mineral nucleation and growth are not highly surface dependent or strictly template-driven. The precipitation is instead promoted by the subtle local pH changes and/or local ion saturation induced by the substrate. Our results suggest that a true template-driven biomineralization process requires the establishment of direct and extensive mineral–substrate contact. High affinity 2-dimensional mineral growth at the substrate–mineral interface observed here reflects such extensive interactions.

We have also shown that external factors such as heating rates, the agitation factor and the duration of the process directly influence the nucleation behavior and extent of mineralization. Avoiding agitation of the HA–urea mineral stock solution during the heating process is essential for promoting the heterogeneous nucleation and mineral growth at the gel–mineral interface. Heating rates between 0.2 °C/min and 0.5 °C/min are appropriate for the formation of a CP layer that uniformly covers the gel surface. Extended mineralization after reaching 95 °C could effectively increase the thickness of the CP layer grown on the gel surface to micron scale. This, along with the strong adhesion at the gel–mineral interface, affords the composites generated here a CP layer with a structure and thickness that are ideal for bone implant applications. Analysis of calcium phosphate coatings on titanium implants has shown that resorption of the coating occurs mostly in the less organized apatite region and stops where the coating has higher crystallinity.[49] Thus, amorphous or nanocrystalline CP coatings as we have achieved should promote resorption and bone integration. In addition, earlier studies suggest that a thin layer of CP with thickness on the order of 1–7 μm, as we have achieved, provides a sufficient CP resorption timeframe to allow a progressive bone contact with the implant substrate, and is therefore ideal for inducing integration of the material into natural bone.[49] The favorable properties of the hydrogel–CP composite obtained using the approach described here may potentially maximize the chance for initiating in vivo remodeling cascades and subsequent positive tissue-implant integration.

More in vitro and in vivo studies will have to be performed before the real value of composites formed using this approach can be estimated. In addition, the porosity of the hydrogel scaffold has not yet been tuned, although many available techniques[16,17,19,21] can be applied to this effort. Such modifications could further enhance the degree of mineralization at the interior of the composite material and allow deeper tissue ingrowth. These applications and extensions of the method are presently under investigation.

Acknowledgements

This work was supported by the Laboratory Directed Research and Development Program of Lawrence Berkeley National Laboratory under the Department of Energy Contract No. DE-AC03-76SF00098.

References

1. Black, J., *Biological Performance of Materials: Fundamentals of Biocompatibility, 3rd rev. and expanded edn*. Marcel Dekker, New York, 1999.
2. Willmann, G., Coating of implants with hydroxyapatite—material connections between bone and metal. *Adv. Eng. Mater*., 1999, **1**, 95–105.
3. Weiner, S. and Wagner, H. D., The material bone: structure mechanical function relations. *Annu. Rev. Mater. Sci*., 1998, **28**, 271–298.
4. Sikavitsas, V. I., Temenoff, J. S. and Mikos, A. G., Biomaterials and bone mechanotransduction. *Biomaterials*, 2001, **22**, 2581–2593.
5. Raj, P. A., Johnson, M., Levine, M. J. and Nancollas, G. H., Salivary statherin. Dependence on sequence, charge, hydrogen bonding potency, and helical conformation for adsorption to hydroxyapatite and inhibition of mineralization. *J. Biol. Chem*., 1992, **267**, 5968–5976.
6. Clark, R. H., Campbell, A. A., Klumb, L. A., Long, C. J. and Stayton, P. S., Protein electrostatic surface distribution can determine whether calcium oxalate crystal growth is promoted or inhibited. *Calcif. Tissue Int*., 1999, **64**, 516–521.
7. Addadi, L. and Weiner, S., Interactions between acidic proteins and crystals: stereochemical requirements in biomineralizaton. *Proc. Natl. Acad. Sci. USA*, 1985, **82**, 4110–4114.

8. George, A., Bannon, L., Sabsay, B., Dillon, J. W., Malone, J., Veis, A., Jenkins, N. A., Gillbert, D. J. and Copeland, N. G., The carboxyl-terminal domain of phosphophoryn contains unique extended triplet amino acid repeat sequences forming ordered carboxyl-phosphate interaction ridges that may be essential in the biomineralization process. *J. Biol. Chem.*, 1996, **271**, 32869–32873.
9. Shea, L. D., Smiley, E., Bonadio, J. and Mooney, D. J., DNA delivery from polymer matrices for tissue engineering. *Nat. Biotechnol.*, 1999, **17**, 551–554.
10. Lee, K. Y., Peters, M. C., Anderson, K. W. and Mooney, D. J., Controlled growth factor release from synthetic extracellular matrices. *Nature*, 2000, **408**, 998–1000.
11. Mann, B. K., Schmedlen, R. H. and West, J. L., Tethered-TGF-beta increases extracellular matrix production of vascular smooth muscle cells. *Biomaterials*, 2001, **22**, 439–444.
12. Luo, Y., Dalton, P. D. and Shoichet, M. S., Investigating the properties of novel poly(2-hydroxyethyl methacrylate-co-methyl methacrylate) hydrogel hollow fiber mmebranes. *Chem. Mater.*, 2001, **13**, 4087–4093.
13. Hartgerink, J. D., Beniash, E. and Stupp, S. I., Self-assembly and mineralization of peptide-amphiphile nanofibers. *Science*, 2001, **294**, 1684–1688.
14. Peppas, N. A., *Hydrogels in Medicine and Pharmacy*. CRC Press, Boca Raton, 1986.
15. Lee, K. Y. and Mooney, D. J., Hydrogels for tissue engineering. *Chem. Rev.*, 2001, **101**, 1869–1879.
16. Holy, C. E., Shoichet, M. S. and Davies, J. E., Engineering three-dimensional bone tissue in vitro using biodegradable scaffolds: investigating initial cell-seeding density and culture period. *J. Biomed. Mater. Res.*, 2000, **51**, 376–382.
17. Mooney, D. J., Cima, L., Langer, R., Johnson, L., Hansen, L. K., Ingber, D. E. and Vacanti, J. P., Principles of tissue engineering and reconstruction using polymer-cell constructs. *Mater. Res. Soc. Symp. Proc.*, 1992, **252**, 345–352.
18. Klawitter, J. J. and Hulbert, S. F., Application of porous ceramics for the attachment of load bearing internal orthopedic applications. *J. Biomed. Mater. Res. Symp.*, 1971, **2**, 161–229.
19. Harris, L. D., Kim, B.-S. and Mooney, D. J., Open pore biodegradable matrices formed with gas foaming. *J. Biomed. Mater. Res.*, 1998, **42**, 396–402.
20. Mikos, A. G., Sarakinos, G., Leite, S. M., Vacanti, J. P. and Langer, R., Laminated three-dimensional biodegradable foams for use in tissue engineering. *Biomaterials*, 1993, **14**, 323–330.
21. Whang, K. and Healy, K. E., Processing of polymer scaffolds: freeze-drying. In *Methods of Tissue Engineering*, ed. A. Atala and R. P. Lanza. Academic Press, San Diego, San Francisco, New York, Boston, London, Sydney, Tokyo, 2002, pp. 697–704.
22. Brauker, J. H., Carr-Brendel, V. E., Martinson, L. A., Crudele, J., Johnston, W. D. and Johnson, R. C., Neovascularization of synthetic membranes directed by membrane microarchitecture. *J. Biomed. Mater. Res.*, 1995, **29**, 1517–1524.
23. Massia, S. P. and Hubbell, J. A., Covalently attached grgd on polymer surfaces promotes biospecific adhesion of mammalian-cells. *Ann. N.Y. Acad. Sci.*, 1990, **589**, 261–270.
24. Barrera, D. A., Zylstra, E., Lansbury, P. T. and Langer, R., Synthesis and rgd peptide modification of a new biodegradable copolymer—poly(lactic acid-co-lysine). *J. Am. Chem. Soc.*, 1993, **115**, 11010–11011.
25. Ratner, B. D., The engineering of biomaterials exhibiting recognition and specificity. *J. Mol. Recognit.*, 1996, **9**, 617–625.
26. Kost, J. and Langer, R.. In *Hydrogels in Medicine and Pharmacy, Vol. III*, ed. N. Peppas. CRC Press, Boca Raton, 1987, pp. 95.
27. Phillips, A. J. and Stone, J., *Contact Lenses*. Butterworth & Co, London, Boston, 1989.
28. Kidane, A., Sxabocsik, J. M. and Park, K., Accelerated study on lysozyme deposition on poly(HEMA) contact lenses. *Biomaterials*, 1998, **19**, 2051–2055.
29. Oxley, H. R., Corkhill, P. H., Fitton, J. H. and Tighe, B. J., Macroporous hydrogels for biomedical applications: methodology and morphology. *Biomaterials*, 1993, **14**, 1064–1072.
30. Vermeiden, J. P. W., Rejda, B. B., Peelen, J. G. J. and de Groot, K., Histological evaluation of calcium hydroxyapatite bioceramics, pure and reinforced with polyhydroxyethylmethacrylate. In *Evaluation of Biomaterials*, ed. G. D. Winter, J. L. Leray and K. de Groot. Wiley, New York, 1980, pp. 405–411.
31. Yang, J. M., You, J. W., Chen, H. L. and Shih, C. H., Calorimetric characterization of the formation of acrylic type bone cements. *J. Biomed. Mater. Res.*, 1996, **33**, 83–88.
32. Prati, C., Mongiorgi, R., Valdre, G. and Montanary, G., Hydroxyethyl-methacrylate Dentin bonding agents: shear bond strength, marginal microleakage and SEM analysis. *Clin. Mater.*, 1991, **8**, 137–143.
33. Lu, S. and Anseth, K. S., Photopolymerization of multilaminated poly(HEMA) hydrogels for controlled release. *J. Controlled Release*, 1999, **57**, 291–300.
34. Sefton, M. V., May, M. H., Lahooti, S. and Babensee, J. E., Making microencapsulation work: conformal coating, immobilization gels and in vivo performance. *J. Controlled Release*, 2000, **65**, 173–186.
35. Kokubo, T., Apatite formation on surfaces of ceramics, metals and polymers in body environment. *Acta Mater.*, 1998, **46**, 2519–2527.
36. Rhee, S.-H. and Tanaka, J., Effect of citric acid on the nucleation of hydroxyapatite in a simulated body fluid. *Biomaterials*, 1999, **20**, 2155–2160.
37. Murphy, W. L. and Mooney, D. J., Bioinspired growth of crystalline carbonate apatite on biodegradable polymer substrata. *J. Am. Chem. Soc.*, 2002, **124**, 1910–1917.
38. Labella, R., Braden, M. and Deb, S., Novel hydroxyapatite-based dental composites. *Biomaterials*, 1994, **15**, 1197–1200.
39. Dupraz, A. M. P., de Wijn, J. R., vander Meer, S. A. T. and de Groot, K., Characterization of silane-treated hydroxyapatite powders for use as filler in biodegradable composites. *J. Biomed. Mater. Res.*, 1996, **30**, 231–238.
40. Misra, D. N., Adsorption of zirconyl salts and their acids on hydroxyapatite: use of the salts as coupling agents to dental polymer composites. *J. Dent. Res.*, 1985, **12**, 1405–1408.
41. Bradt, J.-H., Mertig, M., Teresiak, A. and Pompe, W., Biomimetic mineralization of collagen by combined fibril assembly and calcium phosphate formation. *Chem. Mater.*, 1999, **11**, 2694–2701.
42. Liu, Q., de Wijn, J. R., Bakker, D., van Toledo, M. and van Blitterswijk, C. A., Polyacids as bonding agents in hydroxyapatite polyester-ether (Polyactive (TM) 30/70) composites. *J. Mater. Sci.-Mater. Med.*, 1998, **9**, 23–30.
43. Liu, Q., de Wijn, J. R. and van Blitterswijk, C. A., Covalent bonding of PMMA, PBMA, and poly(HEMA) to hydroxyapatite particles. *J. Biomed. Mater. Res.*, 1998, **40**, 257–263.
44. Liu, Q., de Wijn, J. R. and van Blitterswijk, C. A., A study on the grafting reaction of isocyanates with hydroxyapatite particles. *J. Biomed. Mater. Res.*, 1998, **40**, 358–364.
45. Hsueh, C. H. and Evans, A. G., Residue stresses and cracking in metal/ceramic systems for microelectronics packaging. *J. Am. Ceram. Soc.*, 1985, **68**, 120–127.
46. Chalker, P. R., Bull, S. J. and Rickerby, D. S., A review of the methods for the evaluation of coating-substrate adhesion. *Mater. Sci. Eng.*, 1991, **A140**, 583–592.
47. Zhang, Y. W., Zeng, K. Y. and Thampurun, R., Interface delamination generated by indentation in thin film systems—a computational mechanics study. *Mater. Sci. Eng.*, 2001, **A319-321**, 893–897.

48. Chilkoti, A., Lopez, G. P. and Ratner, B. D., Analysis of polymer surfaces by SIMS. 16. Investigation of surface cross-linking in polymer gels of 2-hydroxyethyl methacrylate. *Macromolecules*, 1993, **26**, 4825–4832.
49. Darimont, G. L., Cloots, R., Heinen, E., Seidel, L. and Legrand, R., In vivo behaviour of hydroxapatite coatings on titanium implants: a quantitative study in the rabbit. *Biomaterials*, 2002, **23**, 2569–2575.
50. Nancollas, G. H. and Zhang, J., Formation and dissolution mechanisms of calcium phosphates in aqueous systems. In *Hydroxyapatite and Related Materials*, ed. P. W. Brown and B. Constantnz. CRC, Boca Raton, 1994, pp. 73.
51. Blendell, J. E., Bowen, H. K. and Coble, R. L., High purity alumina by controlled precipitation from aluminum sulfate solutions. *Am. Ceram. Soc. Bull.*, 1984, **63**, 797–801.
52. De Jonghe, L. C. and He, Y., Composite powder synthesis. In *Ceramic Microstructures: Control at the Atomic Level*, ed. A. P. Tomsia and A. Glaeser. Plenum Press, New York, 1998, pp. 559–565.
53. Timmons, C. O. and Zisman, W. A., Effect of liquid structure on contact angle hysteresis. *J. Colloid Interface Sci.*, 1966, **22**, 165–171.
54. Du, C., Cui, F. Z., Zhang, W., Feng, Q. L., Zhu, X. D. and de Groot, K., Formation of calcium phosphate/collagen composites through mineralization of collagen matrix. *J. Biomed. Mater. Res.*, 2000, **50**, 518–527.
55. Saiz, E., Goldman, M., Gomez-Vega, J. M., Tomsia, A. P., Marshall, G. W. and Marshall, S. J., In vitro behavior of silicate glass coatings on Ti6Al4V. *Biomaterials*, 2002, **23**, 3749–3756.
56. Barrere, F., van Blitterswijk, C. A., de Groot, K. and Layrolle, P., Influence of ionic strength and carbonate on the Ca–P coating formation from SBF X 5 solution. *Biomaterials*, 2002, **23**, 1921–1930.
57. Barrere, F., van Blitterswijk, C. A., de Groot, K. and Layrolle, P., Nucleation of biomimetic Ca-P coatings on Ti6Al4V from a SBF X 5 solution: influence of magnesium. *Biomaterials*, 2002, **23**, 2211–2220.